2010

Doppler weather radar as a meteorite recovery tool

Marc Fries

Jeffrey Fries

The Meteoritical Society

Meteoritics & Planetary Science 45, Nr 9, 1476–1487 (2010)
doi: 10.1111/j.1945-5100.2010.01115.x

Doppler weather radar as a meteorite recovery tool

Marc FRIES[1*] and Jeffrey FRIES[2]

[1]Planetary Science Institute, 1700 E. Fort Lowell Rd., Suite 106, Tucson, Arizona 85719, USA
[2]Air Force Weather Agency/1st Weather Group, Offutt AFB, Nebraska 68113, USA
[*]Corresponding author. E-mail: fries@psi.edu

(Received 27 November 2009; revision accepted 29 July 2010)

Abstract–We report the use of Doppler weather radar as a tool for locating meteorites, both at the time of a fall and from archived radar data. This asset is especially useful for meteorite recovery as it can provide information on the whereabouts of falling meteorites in "dark flight" portion of their descent where information on their flight paths cannot be discerned from more traditional meteorite location techniques such as eyewitness accounts. Weather radar data can provide information from detection in three distinct regimes: (A) direct detection of the rapidly moving, optically bright fireball by distant radars, (B) detection of falling debris to include hand-sample sized rocks, and (C) detection of dust produced by detonation events that can occur tens of minutes and many kilometers laterally removed from the actual fireball locality. We present examples of each, as well as comparisons against man-made debris from a re-entering Soyuz rocket and the Stardust Sample Return Capsule. The use of Doppler weather radar as a supplement to traditional meteorite recovery methods holds the promise of improving both the speed and total number of meteorite recoveries, thereby increasing the number of freshly fallen meteorites for scientific study.

INTRODUCTION

Traditionally, meteorite falls are located by investigators with the aid of interviews with eyewitnesses, data from security camera and other video sources (e.g., Brown et al. 1994), and other techniques such as audible (Wylie 1932) and infrasound detection (Donn and Balachandran 1974; ReVelle 1976). These methods generate the preponderance of available data that describe the location of the meteor while it is optically bright down to an altitude of roughly 20 km above the ground. From this point on, any surviving meteorites cannot currently be observed unless they fall in the immediate vicinity of a person on the ground (i.e., the Monahans chondrite; Gibson et al. 1998) or signify their location by damaging property (Povenmire 1985; Brown et al. 1994). A strewn field's location can be estimated by starting with meteorite positions in the sky recorded by the means described above and then calculating expected flight paths to the ground based on the physics of aerodynamically limited falling bodies (Öpik 1958; Pecina and Ceplecha 1983; Ceplecha 1987; Ceplecha et al. 1998). While this has been successful many times (e.g., McCrosky et al. 1971; Halliday et al. 1981; Borovička and Kalenda 2003; Llorca et al. 2005; Bland et al. 2009), the majority of bright meteor sightings do not produce recovered meteorites. Annually, new meteorite falls are recorded in the Meteoritical Society database at a rate of about 5–10 per year, but there are estimates that this number represents only about 0.1% of the annual meteorite falls that are potentially recoverable (Beech 2003). A need exists to reliably image falling meteorites in their "dark flight" phase, or the portion of their flight between the end of bright optical emission and up to the point where they come to rest on the ground. We report the successful use of Doppler weather radars to constrain a meteorite's strewn field location through direct imaging of the falling fireball debris as well as a descriptive scheme for classifying radar observations. The primary benefit of weather radar observations is that falling meteorite debris can be directly imaged with a high degree of positional accuracy at altitudes >20 km above ground level (AGL) to <1 km AGL depending

on fall characteristics and the timing of measurements by local radars. This represents a fundamental improvement in meteorite recovery techniques that should result in faster, more reliable, and more common recovery of meteorite falls both within the United States and potentially for any region with Doppler radar coverage. Additionally, this technique allows us to study the fall of sub-mm meteorite fragments that typically go unrecovered even in major meteorite falls.

METHODS

Two general types of weather radar operate in the United States, the relatively low-power TV station and airport S-band radars operating at 5 cm wavelength and the higher-power, 10 cm wavelength radars of the National Oceanographic and Atmospheric Administration's (NOAA) NEXRAD national network. TV station radars typically do not make their data publicly available nor do they maintain data archives and this limits their utility for meteorite recovery. However, NEXRAD radars send complete volumetric scans to the National Climatic Data Center in Asheville, North Carolina and these data are freely available to the public via the Internet. NEXRAD data are archived back to 1992, facilitating investigation of recent falls.

NEXRAD Weather Radar Network Description

A network of 159 WSR-88D pulsed Doppler radars (Weather Surveillance Radar 1988—Doppler, commonly referred to as NEXRAD) and shorter-range, 5 cm frequency Terminal Doppler Weather Radars sited at airports provides nearly continuous coverage of the United States. Individual radars are identified using a four-letter code such as KFWS, which designates the NEXRAD radar outside of Ft. Worth, TX. WSR-88D radars operate continuously, transmitting a 10 cm wavelength pulse at 750 kW peak power with a maximum effective range of 460 km. WSR-88D radars sweep their interaction volumes according to preprogrammed volume coverage patterns (VCPs). The default mode is a slowly rotating "clear-air mode," or VCP 32, used to save wear and tear on the radar hardware when no storms are present. VCP 32 generates five 360° sweeps, or "altitude cuts," at set elevation angles every 10 min with lowest three cuts repeated to optimize Doppler measurements. The highest-altitude sweep is performed at 4.5° above horizontal in this mode, which generates an interrogation volume that is approximately 8.4 km above radar level at 100 km from the radar. This 10-min data set is packaged as a single time-stamped package for distribution and analysis. The radars will automatically select an appropriate VCP according to local weather conditions, such as VCP 11 a "precipitation mode" used for rapid updates during severe weather. Precipitation mode generates 14 altitude cuts every 6 min with the lowest two cuts repeated to optimize Doppler measurements and the highest cut performed at 19.5. Radar sweeps are performed starting from lowest elevation angle to highest, and the cone-shaped volume directly above the radar that is not imaged is colloquially referred to as a radar's "cone of silence." This volume is not usable for detection of meteorites, but NEXRAD radars are spaced to maximize overlap so that any given radar's cone of silence should be included in the scans of a nearby radar. This equates to an interrogation volume altitude of about 34.5 km at 100 km distance. For practical purposes, the lowest-altitude cut (0.5° above horizontal) is nearly worthless for detection of meteorites due to reflections from the ground, bugs, birds, and other sources of radar noise. Also, the typically weak signals generated by smaller meteorite events are typically lost in "noise" close to a radar, so the optimal search areas for a given radar tend to be found at elevation angles $>0.5°$ and distances from a radar of greater than approximately 50 km, although this value depends strongly on local weather conditions, radar mode, and various other environmental factors. While the NEXRAD system has been used to track nonweather events including bird migration (O'Bannon 1995) and volcanic eruptions (Hendricks 2006; Schneider et al. 2006), its use as a tool for investigating meteorite falls has not been previously reported.

Data Description and Interpretation

Radar data from the NEXRAD network can be obtained from the U.S. National Climatic Data Center (NCDC) and can be analyzed using several software packages both commercial and provided on a public use license. Depending on the emplacement date of the individual radar, archived data may be available as far back as 1992. Data are available in two formats: level II and level III. Level III data are composed of individual products such as radar reflectivity, Doppler velocity images, or other precalculated interpretations of radar data. Level III data are primarily used because of their small file size and decreased incidence of imaging artifacts. Level II data are composed of semiraw radar data from entire time sequences. When searching for meteorites, level II data are of greater utility than level III because they retain weak signals useful for searching for meteorite signatures. The primary data types used to search for meteorites are radar reflectivity, Doppler velocity and spectral width measurements. Reflectivity

is simply the magnitude of energy reflected by objects from each radar pulse and detected at the radar. The information obtained from reflectivity images amounts to the location and reflectance of objects such as clouds, birds, hail, bugs, and meteorite debris in the interaction volume of the radar. This is the data type typically shown in weather broadcasts. Doppler velocity images are obtained by measurement of Doppler shift in reflected radar energy and describe the movement of objects in the interaction volume of the radar. Used together, reflectivity and velocity images are useful for analyzing the movement of falling meteorite debris. A third principal data type is spectrum width, which is a calculated value that expresses the range of Doppler values retrieved from a given image pixel. Highly turbulent processes, such as atmospheric shear set up by the passage of high-velocity meteorites, tend to produce relatively large values of spectrum width.

Fall and Detection of Meteorite Debris

It is reasonable to expect that both falling meteorites and ablation debris will strongly interact with the WSR-88D radar beam as these radars are optimized to detect the Rayleigh-scattered energy returns from liquid water droplets 0.2 mm and larger. *The American Meteorological Society's Glossary of Meteorology* defines radar reflectivity as, "In general, a measure of the efficiency of a radar target in intercepting and returning radio energy [Reflectivity] depends on the size, shape, aspect, and dielectric properties of the target" (Glickman 2000). Water exhibits a dielectric constant of 0.93, whereas the dielectric constant of forsterite (as a rough analog of ordinary chondrites) is 6.2, asphalt (as a rough analog for carbonaceous chondrites) is 2.7, and iron-nickel is a strongly reflecting conductor (Weast 1973). Therefore, meteorite radar reflectivity should compare favorably with water, at least in terms of their general composition. Further work is required to quantitatively assess actual meteoritic material as well as the effects of typical meteorite shapes and the presence of fusion crust on radar reflectance.

In terms of radar operation, weather radars concern themselves with weather, and so are geometry-limited to interrogate a volume that is generally lower than approximately 20 km AGL, although this parameter varies with the operating mode and scan angle of a given radar. By the time a typical meteor descends to this altitude, it has shed its cosmic velocity and its movement is governed primarily by aerodynamic forces. In other words, the meteor is no longer optically bright and is in the "dark flight" phase of its fall. However, meteorite debris is also detectable at higher altitudes and longer ranges than the radar's designers probably had in mind for weather observation, and these detection events are very useful in identifying meteorite debris. Based on where and when (in the meteor's flight) a radar signal is generated, detection of meteorites will fall into one of three types: (A) high-altitude detection by a distant radar while the meteor is still optically bright, (B) dark flight detection of falling bodies moving at aerodynamically limited speeds, and (C) detection of very small particles potentially carried laterally for many kilometers by winds. The purpose of distinguishing between these types is that the type of radar detection for a given event defines the mathematical treatment necessary to make an estimate of the resulting strewn field's location. Type A events require a lot of luck to detect, as the radar must sweep the volume occupied by the meteor while it is still traveling in the km s^{-1} velocity range and calculation of the resulting strewn field requires inclusion of ablation effects into the dark flight model. Type B events are governed primarily by local winds and so calculating the location and shape of their strewn field is possible using a mathematical treatment of the physics of falling bodies. Type C events are radar detection of fine particles suspended in the atmosphere for tens of minutes, which improves the chances for detection of fine material. Type C events rely on production of a large quantity of fine debris by detonation events and reasonably quiescent weather conditions to prevent widely scattering the fine meteorite debris. Identifying the fall location of meteorites from the location of radar returns of fine particles is a topic that would benefit from further investigation.

Effects of Weather

An advantage of working with data from weather radars is that you get a picture of the weather as context for the falling meteorite debris. Cloud cover, precipitation, and winds aloft at altitudes of up to 50,000′ (15.2 km) are available concurrent to actual radar reflectivity data. Wind velocity and direction in particular can be fed directly into models for the flight path of falling meteorites.

Utilization of Radar Data

Interpretation of radar data is greatly assisted by knowledge of a general search area, the time of the fall, and other factors gleaned through eyewitness interviews, surveillance video imagery, meteor reports available from Internet sites such as the American Meteor Society and other sources. The possibility exists that archived radar data can be "mined" for radar features indicative of falling meteorites, potentially revealing meteorite falls that have occurred in the absence of information from

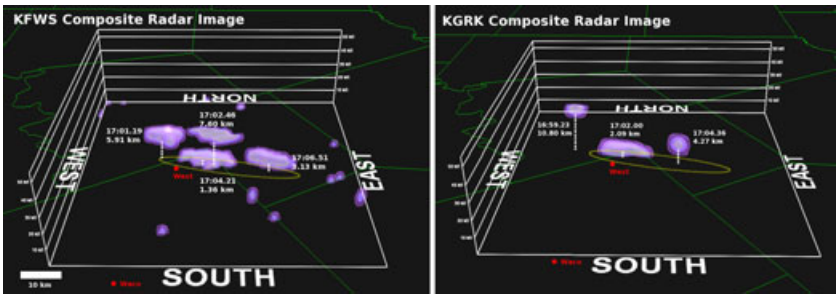

Fig. 1. The Ash Creek meteorite fall outside of West, TX, on February 15, 2009. This set of images shows superimposed images from multiple radar sweeps showing the evolution of falling meteoritic debris in this "type B" event. Two radars produced detailed images of the fall—KFWS 85 km to the north (left image) and KGRK 125 km to the south of the fall (right image). Prominent radar returns shown here occur in individual radar sweeps and are labeled by time and altitude. The estimated strewn field is shown as an ellipse in each image center and radar returns from falling debris are labeled. All times are given in UTC. See online version of this MAPS article for color versions of all figures.

other sources. Software routines are commonly used for identification of radar data patterns that indicate tornadoes and other weather phenomena and it is not beyond reason that similar work could be carried out using the typical features of a meteorite fall event. Such an effort would have to contend with radar noise and other radar anomalies as well as the vast amount of radar data available. The logical sequence of such a search would include the analysis of radar data followed by secondary interpretation of meteorite candidates by an experienced human observer, and then followed by field investigation of promising radar signatures.

RESULTS

The following are examples of type A, B, and C events as well as an example of "space junk" to demonstrate the differences between man-made and natural debris. Radar data from the Stardust Sample Return Capsule (SRC) are also shown to illustrate the effects of "meteoroid" composition on available radar data.

Type A Events

We define type A events as direct radar observations of meteors while they are still optically active and at relatively high altitude. This type of event has not yet been seen, but the likelihood of a type A occurrence is limited only by chance as opposed to technical limitations of the NEXRAD system. While weather radars are not optimized to observe these events as they typically operate at <5° above horizontal so as to observe tropospheric weather phenomena, a portion of each set of radar sweeps does cover altitudes >25 km where direct observation of the fireball may occur. In typical clear-air operating modes, WSR-88D radars observe altitudes >25 km AGL at ranges in excess of 262 km from the radar with the maximum radar range at 460 km. In VCP 11, the WSR-88D interrogates 14 sweeps per data set ranging from 0.5° up to 19.5° above horizontal. Seven of these 14 sweeps occur at 5° or greater where altitudes of >25 km are detected reasonably close to the radar, so >60% of the radar's data set includes nearby airspace at an altitude of >25 km. Timing becomes the major determining factor as to whether or not an active fireball will be detected because the radar antenna must be aimed directly at the meteor to record a radar echo off of the falling body and/or its plasma sheath. As an average fireball lasts only for a few seconds, a type A detection depends heavily on the lucky juxtaposition of the fireball and the radar beam. Even if such an event is recorded, it may actually be less useful than a type B postfireball observation of falling debris as there is far greater uncertainty as to the final resting place of the type A body as it is still moving with a portion of its cosmic velocity. The velocity of the meteorite(s) can be directly measured through Doppler velocity data, but this measurement is a velocity vector whose value is dependent upon the angle of the meteorite's motion relative to the radar beam azimuth. In an extreme example, a meteorite traveling perpendicular to the radar beam would appear to have a velocity of zero. Therefore, any such measurement must be coupled with accurate knowledge of the meteor's direction to calculate properly the actual meteorite's velocity.

Type B Event—The 15 February 2009 Meteorite Fall Near West, TX

We define a type B event as one that produces radar imagery of meteorite material immediately following the fireball and the meteorites themselves are moving at an aerodynamically limited velocity. The Ash Creek meteorite fall outside of the town of West, TX, is

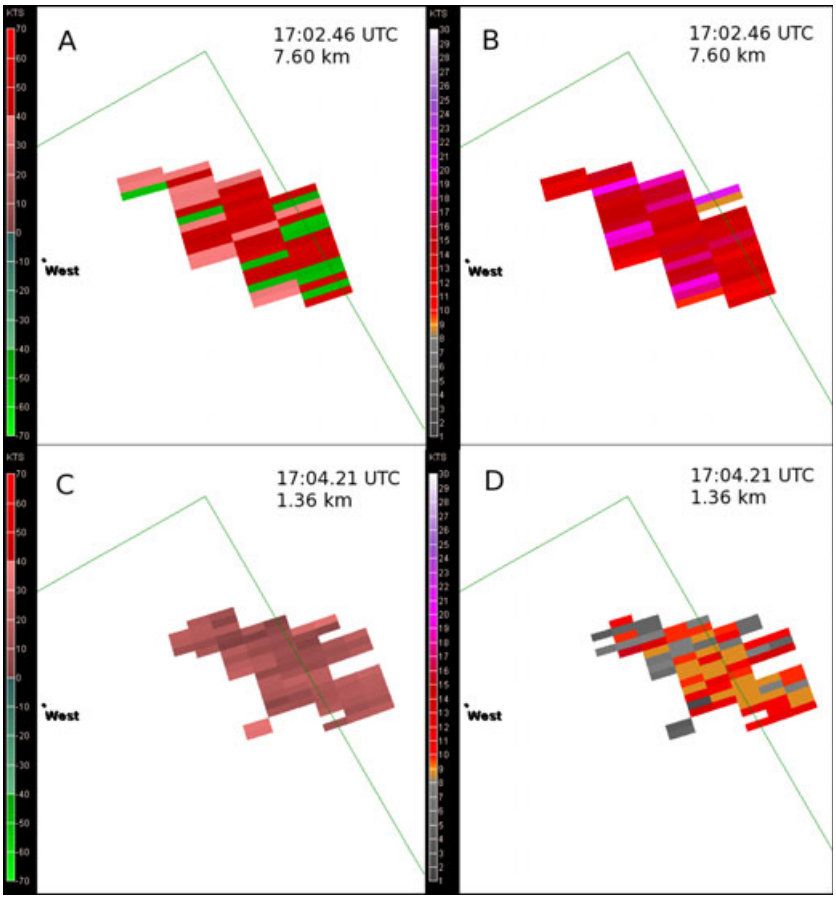

Fig. 2. Horizontal velocity behavior as debris settles in the Ash Creek fall. Velocity data are shown here for the two returns seen in the center of Fig. 1. A) At 7.60 km altitude, significant horizontal shear is seen due to high velocity and deceleration rates of meteoritic debris. Radar data indicate a mixture of debris movement both toward and away from the radar, which is north of the fall (see Fig. 3 for values). Note the appearance of velocities both toward and away from the radar, indicative of wake vortices created by falling material. B) Spectrum width data for the same radar returns as in (A), taken with the velocity data, these are consistent with actual measurements as opposed to data aliasing. C) Falling material in the same location after falling for 95 s. All values are low velocity (6.99 ± 3.36 m s^{-1}) and consistently moving away from the radar (positive values) with the dominant winds out of the WNW, and no wake vortices are seen. D) Spectrum width accompanying velocity data in C, again showing relatively low values indicative of radar reflections from moving targets. At 7.60 km, the meteoritic debris appears to be decelerating, imparting significant turbulence to the surrounding atmosphere. By the time the debris reaches 1.36 km, it has reached a fairly quiescent condition with significantly less horizontal shear. The appearance of wake vorticles may be useful for identifying the flight paths of larger bodies among the falling debris.

the first fireball to produce meteorites and show up on multiple NEXRAD radars, providing the best example to date of a meteorite fall's general appearance in weather radar data. This fall is best classified as a type B fall, as radar imagery shows debris falling immediately following the fireball (Fig. 2). This fall occurred around 1050 local time (1650 UTC) as a bright daytime fireball was observed across central Texas with most meteor reports originating in the Austin and Dallas-Fort Worth metropolitan areas. The meteor was captured on video by a local news crew in Austin and was seen to travel generally from the east to the west. The following day, local news channels carried Doppler weather radar imagery of the fall (Murray 2009; Spencer 2009), and various meteorite hunters later stated that these radar images encouraged a well-attended search on the ground (Sury 2009). While a complete strewn field map is not available at the time of this writing, the combination of site reconnaissance and a partial map of finds provided by a meteorite hunter shows that the strewn field underlies the lowest-altitude images of the debris seen in the radar data. Weather conditions at the time of the fall featured a nearly cloudless day with light winds as revealed by a balloon-borne radiosondes released from Fort Worth by the National Weather Service at 00:00 and 12:00 UTC. Previous work with the Lost City and Park Forest falls demonstrates the strong effect of winds on the final

location of falling meteorites, as Lost City meteorites were found approximately 4 km displaced from a purely ballistic trajectory (McCrosky et al. 1971) and the strewn field of Park Forest wound up nearly perpendicular to the fireball direction due to size-sorting displacement by dominant winds (Brown et al. 2004). While the long axis of the Ash Creek fall lies along the direction of predominant winds, that axis is not far removed from the general direction of the fireball reported by eyewitnesses and recorded on video. This makes the comparison of radar data to the strewn field geometry straightforward.

The Ash Creek fall appears on three different NEXRAD radars. Detailed images appear in data from the Fort Worth, TX, (KFWS) and the Fort Hood, TX, (KGRK) radar northeast of Austin, TX. These radars are approximately 85 and 125 km distant from the strewn field centroid, respectively, and together they straddled the fall site. A weak transient signal also appears on the KEWX radar southwest of Austin at an altitude of 6.2 km at 17:03.30 UTC. This radar is 250 km distant from the strewn field. A fourth radar, KDYX at Dyess AFB, TX, did not produce any images of the fall despite its nearer distance of 225 km. However, this radar operates on a lower spatial resolution data transfer protocol and weak signals may have been further diluted through data binning. The much closer KGRK radar also adheres to the same data protocol and so features lower spatial resolution than the KFWS radar, but is near enough to the fall site to provide useful imagery.

Reflectivity measurements reveal that the falling debris comprised a linear train of particles approximately 20 km long by 2–3 km wide. Two images are presented in Fig. 2; one for each of the two radars (KFWS and KGRK) that were able to spatially resolve the falling meteoritic debris. Figure 2A shows data from KFWS with four significant radar returns that appear over a period of 5 min 32 s. Two radar returns appear to observe material from the center of the strewn field at 7.60 and then 1.36 km altitude. Starting from the assumption that these two radar returns are two different measurements of the same material, we can calculate the approximate mean mass of this material. Starting from the generic equation for terminal velocity (V_T) and assuming all particles are spheres of L chondrite density:

$$V_T = \sqrt{\frac{2mg}{\rho A C_D}}, \quad (1)$$

where m is particle mass (kg); g, acceleration of gravity (9.81 m s^{-2}); ρ, air density (kg m^{-3}); A, particle cross sectional area (m^2); and C_D, drag coefficient. Atmospheric density was calculated using data from a radiosonde balloon launched from Fort Worth at 1200 UTC on the day of the fall and C_D values calculated by iteration using data from Carter et al. (2009). Calculating V_T using the difference in altitude and time recorded for the two radar returns and solving for particle mass gives a value of approximately 80 g, which is a reasonable estimation of the average mass of meteorites recovered from the middle of the Ash Creek strewn field based on publicly reported finds.

These two sequential radar returns also reveal information about the behavior of falling meteorites at low altitude. Horizontal velocities measured from the Doppler shift of radar reflections in Storm Relative Velocity data (i.e., velocity data normalized for ambient winds) (Fig. 3) are probably a mixture of signals originating from both direct reflection from falling meteoritic particles and accompanying radar beam refraction due to disruption of the surrounding atmosphere. At 17:02.46 UTC and 7.60 km altitude (Fig. 3A), measured velocities show a bimodal distribution (Fig. 4) with magnitudes of 21.70 ± 2.66 and −24.54 ± 1.12 m s^{-1} indicating localized horizontal vorticity. This turbulence may indicate that particles are still decelerating at 7.60 km imparting dramatic shear to the local atmosphere. Additionally, the appearance of discernable shear in the radar data indicates that horizontal vorticles appear on a scale comparable to the 0.13 km image pixels in the radar data at this point. The presence of these wake vortices is useful because it may indicate the locations of larger bodies in the falling meteorite debris, and if this hypothesis is true then the appearance of horizontal shear in the velocity data may be useful in identifying the flight paths of larger bodies for subsequent ground search. Terminal velocity for 80 g chondritic spheres at this altitude is 78.4 m s^{-1} or Mach 0.26. Spectrum width measurements (Fig. 3B) show the range of velocities detected for each pixel and in this case denote a broad range of values (mean = 7.1 m s^{-1}), but are generally within the range expected for reflections from particles of varying size and shape and so indicate that the velocity data are real as opposed to a Doppler aliasing artifact. Velocity data for the radar return at 17:04.21 UTC and 1.36 altitude (Fig. 3C) show no horizontal shear relative to the 7.60 km data with fairly uniform drift away from the radar at about 6 m s^{-1} (Fig. 4). The radar is toward the north and predominant winds are out of the WNW near 270° through the entire local atmosphere up to the 9.1 km altitude upper limit of available winds data, so drift away from the radar is probably a vector component of particle drift with the prevailing winds. As an aside, the long axis of the Ash Creek strewn field follows closely the dominant wind direction, so the

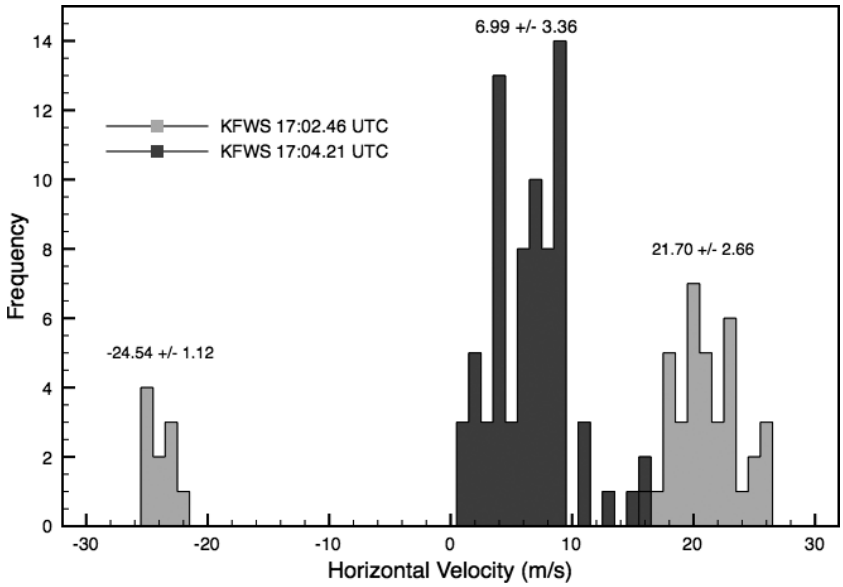

Fig. 3. Velocity distribution evolution. Histograms of velocity data from (A) black bars and (B) gray bars. Note that the 17:02.46 UTC data from 7.60 km show bimodal behavior with values of 21.70 ± 2.66 and −24.54 ± 1.12 m s^{-1} implying general movement away from the radar with a horizontal vorticity component. The 17:94.21 UTC shows relatively shear-free, nearly uniform movement away from the radar at less than half the velocity magnitude of the 7.60 km data. The change in velocity relative to the radar is attributed to wind velocity variation with altitude.

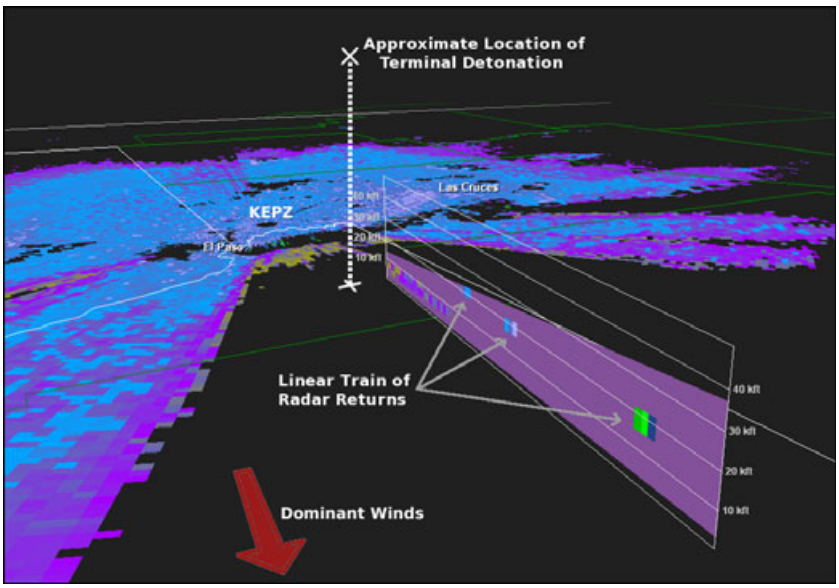

Fig. 4. Small debris falling from the El Paso ''superbolide'' of October 09, 1997. A perspective view of a cross section through composite radar data showing three radar returns from fine debris originating from the high-altitude superbolide detonation. This illustrates ''type C'' radar detection of dust-sized material. The three returns occur approximately 38 min after the detonation and constitute three points in three different radar sweeps where the radar beam intersects a linear chain of fine, slowly settling debris that have been transported toward the east by prevailing winds. The KEPZ NEXRAD radar is located at the center of the fan-shaped radar ''noise.''

''direction'' of this strewn field is dominated by local winds as opposed to the path of the fireball itself. This observation, coupled with the radar observations of falling debris moving with the dominant winds (Fig. 3), indicates that perhaps strewn field shape is generally only loosely coupled with fireball direction. This finding is in agreement with the shape of the strewn field of the Park Forest, IL meteorite fall, which was nearly perpendicular to the direction of the fireball but lines up along the dominant wind flow (Brown et al.

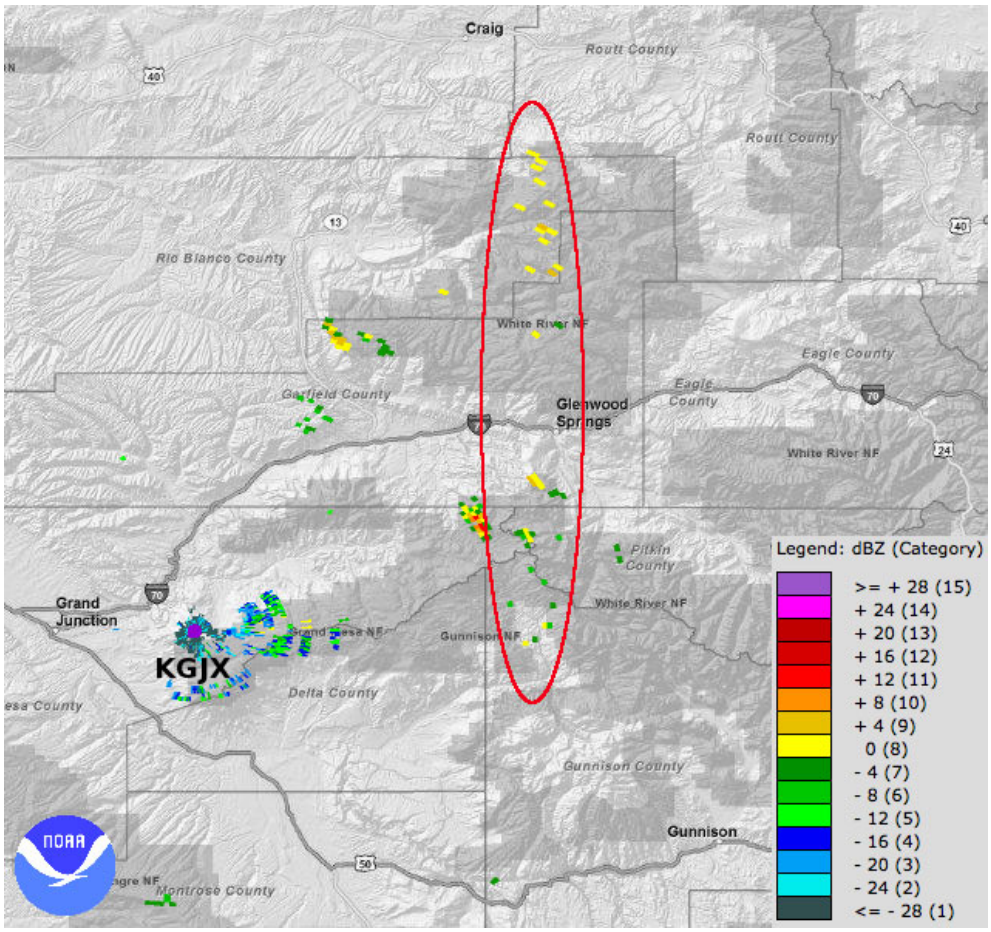

Fig. 5. Soyuz booster debris over Colorado. On January 04, 2007, an upper stage of the Soyuz booster that placed the French CoRoT telescope in orbit deorbited over western Colorado. The booster approached out of the north on a north-south polar orbit, strewing debris over an approximately 140 km long path (ellipse). The KGJX radar in Grand Junction, CO tracked some individual pieces of debris to <1 km AGL, but at the time of this writing none have been recovered. The labels on this image are county names, the KGJX radar site, and the city of Grand Junction, CO.

2004). Spectrum width analysis (Figs. 3B and 3D) shows that the range of velocity values measured for each pixel has decreased in magnitude to nearly half the 7.60 km value (mean = 6.99 ± 3.36 m s^{-1}). Terminal velocity at 1.36 km as described above is 56.7 m s^{-1} or Mach 0.17. Taken together, data from these presumably paired returns show decreasing localized turbulence as the meteoritic debris decelerates through its vertical travel.

A perusal of the times and altitudes of the various radar detections by both KWFS and KGRK (Fig. 2) reveals a complicated pattern. The first detection is at 16:59.23 UTC in the KGRK data and is located to the west of the approximate strewn field, which in turn is based on a compilation of reported find locations. This implies but does not guarantee that additional meteorites may have landed in this area. The prominent return in the center of the strewn field in the KGRK data actually occurs 46 s before the KFWS returns in the same spot at 7.60 km. A possible explanation is that some vertical size sorting occurred and the KGRK return is composed of larger meteorites than the smaller debris which appear later in the KFWS data. This explanation would require doing away with the seemingly valid 80 g average mass estimate described above, however.

Type C Event—El Paso "Superbolide" of October 09, 1997

The El Paso "superbolide" in 1997 provides an example of a type C event. This superbolide has been thoroughly documented (Hildebrandt et al. 1999) and was remarkable for its optical intensity, with eyewitnesses reporting that it cast shadows around noon (1847:15 UTC) on a cloudless west Texas day. Despite a thorough examination of evidence and extensive ground search, no meteorites have been recovered as of yet, but

the capability to retrieve and analyze NEXRAD radar from this event underlines the utility of this technique for re-examining recent prospective falls.

Radar data in this event do not appear to show a direct detection of large, falling meteorite debris. This is simply a matter of timing; two radars were in range to observe the event closely but neither happened to sweep the volume occupied by "large" meteorites before they reached the ground. Small debris, however, can drift a considerable distance from the site of the fireball. In the El Paso event, a linear chain of three very strong radar returns appeared downwind of the superbolide detonation point about 38 min after the event (Fig. 4). Atmospheric pressure and temperature from a NOAA radiosonde balloon released from Midland, TX, on the same day provide an atmospheric density profile reasonably near that of the El Paso area. Using the general equation for terminal velocity and assuming that spherical particles of L chondrite density are moving at this speed, we calculate that particles with settling time to local ground level of 38 min would have a mass of 0.04 mg, corrected for wind drift and from an altitude of 28.5 km. This is the superbolide detonation altitude quoted in Hildebrand et al. (1999). Such particles are approximately 300 m in diameter and photographic evidence suggests (Hildebrand et al. 1999) that they were produced in large quantities during the superbolide event. They are also of sufficient size to show up reliably in NEXRAD radar data as shown from observations of volcanic ash (Marzano et al. 2006), so it is reasonable to assign a meteoritic origin to the linear chain of radar returns. From this point, the outstanding challenge of type C events is to produce a calculated position of meteorites on the ground from radar reflections produced by slowly falling dust-sized debris.

"Space Junk" Re-Entry—Soyuz Second Stage over Colorado on January 04, 2007

Examination of radar images from man-made re-entry debris allows us to discriminate between this type of event and natural meteorite falls in radar data. An example of man-made debris was provided around 13:10 UTC on January 04, 2007, when a bright but slowly moving trail of debris appeared over Wyoming and moved south over western Colorado. Many eyewitness reports were recorded with local news stations, police, and meteor-related websites. Cameras on board a local TV station's helicopter in Denver and all-sky meteor cameras in the area recorded most of the event, which shows the object fragment into many pieces over a period of over 40 s. Soon afterward the North American Aerospace Defense Command (NORAD) released a press statement identifying the object as the 2355 kg (dry mass) upper stage of a Russian Soyuz 2.1b launcher that had placed the French CoRoT space telescope in orbit 8 days previously (Atkins 2007). Technically, this event qualifies as a type B event with a large number of debris tracked from altitudes of 15.3 down to 1.8 km AGL. These objects differ from meteoritic debris in that they include a large number of angular pieces of metal, which tends to produce more intense radar reflections than rounded, silicate-rich meteorite debris. Also, the Soyuz stage was moving at only 8 km s^{-1} on atmospheric entry (Peterson 2007) where natural meteors typically feature much higher entry velocities. The lower velocity, coupled with a shallow entry angle, prolonged the falling body's breakup and produced a much longer field of falling debris than is seen in meteorite falls.

The Doppler weather radar in Grand Junction, Colorado (KGJX) happened to lie very near to the ground track of the falling rocket. KGJX radar data show (Figure 5) the evolution of many individual returns along a linear trace that covers almost the entire width of the radar's search area and differs from the highly localized returns of a meteorite event. Radar returns appear at 1327:38 UTC at 15.3–3.7 km altitude along a track over 200 km long (Fig. 6). One object in particular appears at the far northern end of the track and produces a large field of individual, bright radar returns. This object features strong radar reflectivity. It is also apparently a low-density object as it separated from the rocket early on and may be a shroud or some other metallic debris with large surface area. Debris from this object can be tracked in some cases down to 1.8 km altitude. Other returns appear as point sources scattered over the length of the track and probably represent small metallic fragments of the Soyuz booster. Objects are seen to drift toward the east over a period of approximately 22 min and the last objects disappear from view after the 13:49 UTC radar sweep. Overall, this man-made object is readily discernable from the Ash Creek fall because it covers a much longer strewn field (>200 versus 20 km for Ash Creek) and features falling objects with dramatically different fall behaviors.

The Stardust Sample Return Capsule

The SRC returned to Earth at 10:04 UTC, January 15, 2006. The SRC landed in Dugway Proving Ground, Utah, carrying aerogel-embedded fragments of comet 81P/Wild 2 (Brownlee et al. 2006). The SRC's ground track passed within 250 km of six NEXRAD radars, but the SRC itself only descended below 30 km AGL

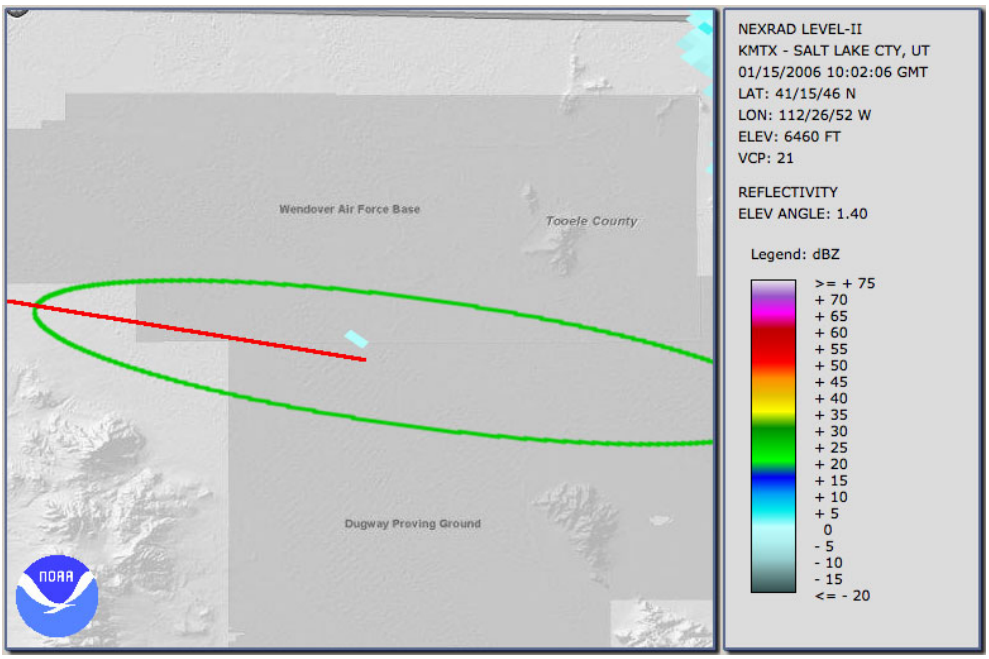

Fig. 6. The Stardust Sample Return Capsule (SRC). Radar imagery from the KMTX radar (out of the image at upper right) showing the Stardust SRC 3.2 km above local ground level during its landing. The SRC is the single black pixel at the center of the image, seen at 10:03.39 UTC on January 15, 2006. The black ellipse is the estimated landing ellipse and the gray arrow is the ground track for the SRC as calculated by the recovery team. Local winds below 20 km AGL are out of a compass heading of 220° at an average velocity of 20 m s^{-1}, which makes detection of the SRC north of the calculated landing approach track reasonable.

within approximately 20 km of its landing site (Jenniskens et al. 2005) and within the interaction volume of a single radar—the KMTX radar outside of Salt Lake City, UT. A single-pixel radar return consistent with detection of the SRC appears at 10:03.09 UTC and an altitude of 3.2 km AGL over the Dugway Proving Ground, UT (Fig. 6). No other radar returns are recorded within 43 km of this return. This radar return occurs at a time consistent with the SRC re-entry for that altitude and the 2.5 × 1 km image pixel is located approximately 5 km downwind of a ballistic ground track calculated for the SRC by the recovery team. Therefore, the time, spatial location and altitude are all reasonable to identify this radar return as the falling SRC. At the time of the radar detection, the SRC was descending under its drogue parachute but the main parachute had not yet opened (Vellinga, personal communication). Of special importance is the fact that the radar signature of the SRC is confined to a single image pixel. The Phenolic Impregnated Carbon Ablator (PICA) heat shield of the SRC is designed to lose mass by oxidative sublimation rather than by debris production and so did not produce particles suitable for radar detection (Kontinos et al. 2008). The fact that observation of the SRC is confined to a single pixel is a consequence of the fact that no significant debris was generated by the capsule.

DISCUSSION

Radar detection of falling meteorites and fine debris includes an element of serendipity. With currently available technology, meteorite radar returns are distinguishable from clouds based mainly on their behavior more than by characteristics of the radar signal itself. These signature features can be summarized as such:

Movement

Clouds tend to move laterally with the prevailing winds, while meteorite debris falls through sequentially lower altitude cuts in the radar data with relatively little lateral movement. Meteoritic debris are seen to sort themselves along the prevailing winds in the Ash Creek fall, in agreement with similar observations made in the Park Forest fall (Brown et al. 2004).

Shape

Meteorite debris is shed from the fireball along the length of its track, resulting in a pronounced oblong signature that can form a linear track between multiple altitude cuts. Rain, snow, and other precipitation tend to appear in multiple radar sweeps as a feature with vertical

depth, whereas meteorite debris tends to appear along linear tracks that appear sequentially in lower altitude cuts. The length of meteorite returns also tends to be limited to around 25 km long as opposed to much longer strewn fields produced by slower-moving "space junk."

Velocity

Doppler radar data indicate that sizable falls such as Ash Creek generate significant horizontal shear within the falling debris cloud and that this turbulence attenuates as altitude (and vertical velocity) decreases. Both velocity and spectrum width signatures became weak and relatively uniform by the time they appear in the 0.5° radar sweep, limiting the possibility of using these features to discern falling meteoritic debris in this typically "noisy" sweep.

Optimally, radar signatures for meteorite debris should appear in sequentially lower altitude cuts, appear at the same location in images from multiple radars if they happen to overlap, and describe an ellipse approximately 25 × 5 km in size (based on Ash Creek). Alternatively, they may appear at altitudes that are not reasonable for weather phenomena at a time and location corroborated by other methods such as eyewitness accounts or video capture.

Where to Go From Here

Given additional work, it should be possible to produce an estimate of the amount of meteorite material that reaches the ground in a given fall from weather radar data. This estimate is not straightforward, as it will vary with nonlinear radar reflectance versus particle size effects, the reflectivity of exposed meteorite material (i.e., fusion crust versus fractured surfaces), radar propagation effects given the local weather conditions, interference from weather, distance from the observing radar, and variation in the size distribution of falling meteorites due to fall dynamics. Once a method is derived to come up with such an estimate, testing the efficiency of the method will rely on comparison against meteorites recovered from radar-observed falls. This in turn will be affected by the many vagaries associated with meteorite recovery. Still, it should be possible to generate an estimate for the amount of material in a radar-observed fall once sufficient empirical data are available. The fact that NOAA radar data are freely available should encourage individuals from a broad range of backgrounds to learn this technique. It is quite likely that this technique will evolve into the hands of the hobbyist, producing useful tools to assist nonspecialists in the rapid recovery of meteorites and discovery of recent falls from archived data. Additionally, the authors hope that national radar networks elsewhere in the world will follow the NOAA example, archiving their data and making them freely available. The result is that significantly more meteorites should become available for scientific investigation, classroom study, and for display in museums around the world.

Acknowledgments—M. Fries extends thanks Tony and Carolyn Mabile of the Lucky 6 Farm and Ranch, West, TX, for their guided tour of the Ash Creek strewn field, and to Mike Miller of Kingman, AZ, for his list of meteorite find coordinates from that fall. The assistance of Marvin Killgore, David Gheesling, and Darryl Pitt is also greatly appreciated. The authors also acknowledge Mr. Jason Dunn of the National Weather Service, who independently noted the appearance of the Ash Creek meteorite fall in radar data at the time of the fall. The authors respectfully dedicate this work to the STS-107 crew of the Space Shuttle Columbia.

Editorial Handling—Dr. Donald Brownlee

REFERENCES

Atkins W. 2007. *Pieces of Soyuz-2.1b (rather than SL-4) rocket fall on Wyoming after launch of Corot satellite*. http://www.itwire.com/science-news/space/8395-pieces-of-soyuz-21b-rather-than-sl-4-rocket-fall-on-wyoming-after-launch-of-corot-satellite (January 05, 2007). Accessed June 16, 2010.

Beech M. 2003. Canadian fireball rates and meteorite falls—declining returns? *Meteorite* 9:4.

Bland P., Spurný P., Towner M., Bevan A., Singleton A., Bottke W., Greenwood R., Chesley S., Shrben L., Borovička J., Ceplecha Z., McClafferty T., Vaughan D., Benedix G., Deacon G., Howard K., Franchi I., and Hough R. 2009. An anomalous basaltic meteorite from the innermost main belt. *Science* 325:1525–1527.

Borovička J. and Kalenda P. 2003. The Morávka meteorite fall: 4. Meteoroid dynamics and fragmentation in the atmosphere. *Meteoritics & Planetary Science* 38:1023–1043.

Brown P., Ceplecha Z., Hawkes R., Wetherill G., Beech M., and Mossman K. 1994. The orbit and atmospheric trajectory of the Peekskill meteorite from video records. *Nature* 367:624–626.

Brown P., Pack D., Edwards W., ReVelle D., Yoo B., Spalding R., and Tagliaferri E. 2004. The orbit, atmospheric dynamics, and initial mass of the Park Forest meteorite. *Meteoritics & Planetary Science* 39:1781–1796.

Brownlee D., Tsou P., Aléon J., Alexander C. M. O'D., Araki T., Bajt S., Baratta G. A., Bastien R., Bland P., Bleuet P., Borg J., Bradley J. P., Brearley A., Brenker F., Brennan S., Bridges J. C., Browning N., Brucato J. R., Brucato H., Bullock E., Burchell M. J., Busemann H., Butterworth A., Chaussidon M., Cheuvront A., Chi M., Cintala M. J., Clark B. C., Clemett S. J., Cody G., Colangeli L., Cooper G., Cordier P. G., Daghlian C., Dai Z., D'Hendecourt L., Djouadi Z., Dominguez G., Duxbury T., Dworkin J. P., Ebel D., Economou T. E., Fairey S. A. J., Fallon S., Ferrini G., Ferroir T., Fleckenstein H., Floss C., Flynn

G., Franchi I. A., Fries M., Gainsforth Z., Gallien J.-P., Genge M., Gilles M. K., Gillet P., Gilmour J., Glavin D. P., Gounelle M., Grady M. M., Graham G. A., Grant P. G., Green S. F., Grossemy F., Grossman L., Grossman J., Guan Y., Hagiya K., Harvey R., Heck P., Herzog G. F., Hoppe P., Hörz F., Huth J., Hutcheon I. D., Ishii H., Ito M., Jacob D., Jacobsen C., Jacobsen S., Joswiak D., Kearsley A. T., Keller L., Khodja H., Kilcoyne A. L. D., Kissel J., Krot A., Langenhorst F., Lanzirotti A., Le L., Leshin L., Leitner J., Lemelle L., Leroux H., Liu M.-C., Luening K., Lyon I., MacPherson G., Marcus M. A., Marhas K., Matrajt G., Meibom A., Mennella V., Messenger K., Mikouchi T., Mostefaoui S., Nakamura T., Nakano T., Newville M., Nittler L. R., Ohnishi I., Ohsumi K., Okudaira K., Papanastassiou D. A., Palma R., Palumbo M. O., Pepin R. E., Perkins D., Perronnet M., Pianetta P., Rao W., Rietmeijer F., Robert F., Rost D., Rotundi A., Ryan R., Sandford S. A., Schwandt C. S., See T. H., Schlutter D., Sheffield-Parker J. A., Simionovici S., Sitnitsky S. I., Snead C. J., Spencer M. K., Stadermann F. J., Steele A., Stephan T., Stroud R., Susini J., Sutton S. R., Taheri M., Taylor S., Teslich N., Tomeoka K., Tomioka N., Toppani A., Trigo-Rodríguez J. M., Troadec D., Tsuchiyama A., Tuzolino A. J., Tyliszczak T., Uesugi K., Velbel M., Vellenga J., Vicenzi E., Vincze L., Warren J., Weber I., Weisberg M., Westphal A. J., Wirick S., Wooden D., Wopenka B., Wozniakiewicz P. A., Wright I., Yabuta H., Yano H., Young E. D., Zare R. N., Zega T., Ziegler K., Zimmerman L., Zinner E., and Zolensky M. 2006. Comet Wild 2 under a microscope. *Science* 314:1711–1716.

Carter R., Jandir P., and Kress M. 2009. Estimating the drag coefficients of meteorites for all Mach number regimes (abstract #2059). 15th Lunar and Planetary Science Conference. CD-ROM.

Ceplecha Z. 1987. Geometric, dynamic, orbital and photometric data on meteoroids from photographic fireball networks. *Bulletin of the Astronomical Institutes of Czechoslovakia* 38:222–234.

Ceplecha Z., Borovička J., Elford W., ReVelle D., Hawkes R., Porubčan C., and Simek M. 1998. Meteor phenomena and bodies. *Space Science Reviews* 84:327–471.

Donn W. and Balachandran N. 1974. Meteors and meteorites detected by infrasound. *Science* 185:707–709.

Gibson E., Zolensky M., Lofgren G., Lindstrom D., Morris R., and Schmidt S. 1998. Monahans (1998) H5 chondrite: An unusual meteorite fall with extraterrestrial halite and sylvite (abstract). *Meteoritics & Planetary Science* 33:A57–A58.

Glickman T. ed. 2000. *American Meteorological Society Glossary of Meteorology*, 2nd ed. http://amsglossary.allenpress.com/glossary. Accessed July 08, 2010.

Halliday I., Griffin A., and Blackwell A. 1981. The Innisfree meteorite fall: A photographic analysis of fragmentation, dynamics and luminosity. *Meteoritics* 16:153–170.

Hendricks T. 2006. Early detection of the 5 April 2005 Anatahan volcano eruption using the Guam WSR-88D. *NWA Electronic Journal of Operational Meteorology*, 2006-EJ8. http://www.nwas.org/ej/pdf/2006-EJ8.pdf. Accessed November 23, 2009.

Hildebrandt A., Brown P., Crawford D., Boslough M., Chael E., ReVelle D., Doser D., Tagliaferri E., Rathbun D., Cooke D., Adcock C., and Karner J. 1999. The El Paso Superbolide of October 9, 1997 (abstract). *30th Lunar and Planetary Science Conference*. p. 1525.

Jenniskens P., Wercinski P., Wright M., Olejniczak J., Raiche G., Koritinos D., Schilling E., Rossano G., Russell R., Taylor M., Stenbaek-Nielsen H., McHarg G., Spalding R., Sandquist K., Hatton J., Abe S., Rairden R., ReVelle D., and Gural P. 2005. Hyperseed MAC: An airborne and ground-based campaign to monitor the Stardust Sample Return Capsule reentry on 2006 January 15. *Dust in Planetary Systems: Workshop Program and Abstracts* 1280:79–80.

Kontinos D., Ellerby D., Milos F., Cozmuta I., Arnold J., Lavelle J., and Stackpoole M. 2008. Post-flight evaluation of Stardust PICA forebody heatshield material. 6th International Planetary Probe Workshop.

Llorca J., Trigo-Rodríguez J., Ortiz J., Docobo J., Garcia-Guinea J., Castro-Tirado A., Rubin A., Eugster O., Edwards W., Laubenstein M., and Casanova I. 2005. The Villalbeto de la Peña meteorite fall: I. Fireball energy, meteorite recovery, strewn field, and petrography. *Meteoritics & Planetary Science* 40:785–804.

Marzano S., Barbieri S., Vulpiani G., and Rose W. 2006. Volcanic ash cloud retrieval by ground-based microwave weather radar. *IEEE Transactions on Geoscience and Remote Sensing* 44:3235–3246.

McCrosky R., Posen A., Schwartz G., and Shao C. 1971. Lost City meteorite—Its recovery and a comparison with other fireballs. SAO Special Report 336.

Murray M. 2009. *Meteor captured on radar*. Austin, Texas: KVUE News. http://www.beloblog.com/KVUE_Blogs/weatherblog/2009/02/meteor-captured-on-radar.html. Accessed June 15, 2009.

O'Bannon T. 1995. Anomalous WSR-88D wind profiles—Migrating birds? 27th Conference on Radar Meteorology. pp. 663–665.

Öpik E. 1958. *Physics of meteor flight in the atmosphere*. Mineola, New York: Dover Publications.

Pecina P. and Ceplecha Z. 1983. New aspects in single-body meteor physics. *Bulletin of the Astronomical Institutes of Czechoslovakia* 34:102–121.

Peterson C. 2007. *January 4, 2007 Fireball*. http://www.cloudbait.com/science/fireball20070104.html. Accessed June 16, 2010.

Povenmire H. 1985. The Claxton, Georgia, meteorite. *Meteoritics* 20:541–544.

ReVelle D. 1976. On meteor-generated infrasound. *Journal of Geophysical Research, Space Physics* 81:1217–1230.

Schneider D., Scott C., Wood J., and Hall T. 2006. NEXRAD weather radar observations of the 2006 Augustine volcanic eruption clouds (abstract V51C-1686). *Eos Transactions, American Geophysical Union* 87:52.

Spencer J. 2009. *Sunday fireball seen on radar*. Austin, Texas: KXAN News. http://blogs.kxan.com/weather/2009/02/16/Sunday-fireball-seen-on-radar/. Accessed June 15, 2009.

Sury K. 2009. Meteorite hunters searching near West find what they believe was part of Sunday's rumble and flash in the sky. *The Waco Tribune* (online). http://www.wacotrib.com/search/content/news/stories/2009/02/19/02192009wacmeteorhunters.html. Accessed June 15, 2009.

Weast R., ed. 1973. *CRC handbook of chemistry and physics*, 53rd ed. Cleveland, Ohio: The Chemical Rubber Co.

Wylie C. 1932. Sounds from meteors. *Popular Astronomy* 40:289.